within the range of the 5800 Å bands; unfortunately, it has yet to be observed in the gas phase. The failure to detect C_3 in absorption in diffuse clouds (*24*), however, appears to rule out this attribution.

Note added in proof: We recently received a manuscript by R. J. Glinski and J. A. Nuth (*27*) in which a vibrational band assignment of the 5800 Å Red Rectangle emission features to C_3 is presented. Combining this assignment with the results described here leads to the conclusion that C_3 is the carrier of the $\lambda = 5797$, $\lambda = 5850$, and nearby related diffuse interstellar absorption bands.

REFERENCES AND NOTES

1. G. H. Herbig, *Astrophys. J.* **196**, 129 (1975); ——— and K. D. Leka, *ibid.* **382**, 193 (1991), and references therein; P. Jenniskens and F.-X. Désert, *Astron. Astrophys. Suppl. Ser.* **106**, 39 (1994).
2. B. E. Westerlund and J. Krełowski, *Astron. Astrophys.* **189**, 221 (1988); *ibid.* **203**, 134 (1988).
3. P. J. Sarre, *Nature* **351**, 356 (1991).
4. S. J. Fossey, *ibid.* **353**, 393 (1991).
5. S. M. Scarrott, S. Watkin, J. R. Miles, P. J. Sarre, *Mon. Not. R. Astron. Soc.* **255**, 11p (1992).
6. N. K. Rao and D. L. Lambert, *ibid.* **263**, L27 (1993).
7. G. D. Schmidt, M. Cohen, B. Margon, *Astrophys. J.* **239**, L133 (1980).
8. R. F. Warren-Smith, S. M. Scarrott, P. Murdin, *Nature* **292**, 317 (1981).
9. G. D. Schmidt and A. N. Witt, *Astrophys. J.* **383**, 698 (1991).
10. H. Van Winkel, C. Waelkens, L. B. F. M. Waters, *Astron. Astrophys.* **293**, L25 (1995).
11. M. L. Sitko, *Astrophys. J.* **265**, 848 (1983).
12. S. P. Balm and M. Jura, *Astron. Astrophys.* **261**, L25 (1992); D. I. Hall, J. R. Miles, P. J. Sarre, S. J. Fossey, *Nature* **358**, 629 (1992).
13. A. N. Witt and T. A. Boroson, *Astrophys J.* **355**, 182 (1990).
14. R. W. Russell, B. T. Soifer, S. P. Willner, *ibid.* **220**, 568 (1978), and references therein.
15. D. G. Furton and A. N. Witt, *ibid.* **415**, L51 (1993); K. Sellgren, in *Dusty Objects in the Universe*, E. Bussoletti and A. A. Vittone, Eds. (Kluwer Academic, Dordrecht, Netherlands, 1990), pp. 35–47.
16. J. Krełowski and G. A. H. Walker, *J. R. Astron. Soc. Can.* **80**, 274 (1986); *Astrophys. J.* **312**, 860 (1987).
17. G. Chlewicki *et al.*, *Astron. Astrophys.* **173**, 131 (1987).
18. P. Jenniskens and F.-X. Désert, *ibid.* **274**, 465 (1993).
19. J. Krełowski and C. Sneden, *Publ. Astron. Soc. Pac.* **105**, 1141 (1993).
20. A spectroscopic interpretation and modeling of these data will be described elsewhere (J. R. Miles, S. M. Scarrott, P. J. Sarre, in preparation).
21. G. P. Van der Zwet and L. J. Allamandola, *Astron. Astrophys.* **146**, 76 (1985); A. Léger and L. B. d'Hendecourt, *ibid.*, p. 81.
22. A. E. Douglas, *Nature* **269**, 130 (1977); J. K. G. Watson, *Astrophys. J.* **437**, 678 (1994).
23. P. D. Bennett, *Bull. Am. Astron. Soc.* **19**, 761 (1987).
24. T. P. Snow, C. G. Seab, C. L. Joseph, *Astrophys. J.* **335**, 185 (1988).
25. G. H. Herbig, personal communication.
26. ———, *Annu. Rev. Astron. Astrophys.*, in press.
27. R. J. Glinski and J. A. Nuth, in preparation.

28. We thank the Panel for the Allocation of Telescope Time for observing time on the Anglo-Australian Telescope and J. Bailey for assistance with the observations. The work of J.R.M. was funded under a fellowship of the Particle Physics and Astronomy Research Council. We thank R. J. Glinski and J. A. Nuth for sending us a copy of their manuscript and G. H. Herbig for permission to reproduce the diffuse absorption band spectrum in Fig. 1.

13 March 1995; accepted 23 May 1995

Decadal Trends in the North Atlantic Oscillation: Regional Temperatures and Precipitation

James W. Hurrell

National Center for Atmospheric Research, P.O. Box 3000, Boulder, CO 80307, USA.

Greenland ice-core data have revealed large decadal climate variations over the North Atlantic that can be related to a major source of low-frequency variability, the North Atlantic Oscillation. Over the past decade, the Oscillation has remained in one extreme phase during the winters, contributing significantly to the recent wintertime warmth across Europe and to cold conditions in the northwest Atlantic. An evaluation of the atmospheric moisture budget reveals coherent large-scale changes since 1980 that are linked to recent dry conditions over southern Europe and the Mediterranean, whereas northern Europe and parts of Scandinavia have generally experienced wetter than normal conditions.

A major source of interannual variability in the atmospheric circulation is the North Atlantic Oscillation (NAO) (*1*), which is associated with changes in the surface westerlies across the North Atlantic onto Europe (*2*). An index of the NAO reveals its variability since 1864 (Fig. 1A). The changes in circulation associated with changes in the NAO index are determined from the difference in sea-level pressure (SLP) between winters with an index value greater than 1.0 and those with an index value less than −1.0 (Fig. 1B). Differences of more than 15 mbar occur across the North Atlantic, with higher than normal pressures south of 55°N and a broad region of anomalously low pressure across the Arctic. During high NAO winters, the westerlies onto Europe are over 8 m s^{-1} stronger than during low NAO winters (Fig. 1B), anomalous southerly flow occurs over the eastern United States, and anomalous northerly flow occurs across western Greenland, the Canadian Arctic, and the Mediterranean.

In addition to interannual variability, there have been several periods (Fig. 1A) when such anomalous circulation patterns persisted over many winters. In the region of the Icelandic low, seasonal pressures were anomalously low during wintertime from the turn of the century until about 1930, while pressures were higher than normal at lower latitudes. Consequently, the wind across the North Atlantic had a strong westerly component, and the moderating influence of the ocean contributed to warmer than normal winter temperatures over much of Europe (*3*). From the early 1940s until the early 1970s, when the NAO index exhibited a downward trend, European wintertime temperatures were frequently lower than normal (*4*, *5*). A sharp reversal has occurred over the past 25 years, with unprecedented strongly positive NAO index values since 1980 and with SLP anomalies much like those shown in Fig. 1B. The 1983, 1989, and 1990 winters were marked by the highest positive values of the NAO index recorded since 1864.

Variations in the quasistationary planetary waves in the atmosphere, among other factors, produce spatially coherent large-scale patterns of anomalies in local surface variables on interannual and longer time scales (*4*, *6*). Such patterns can be observed in the surface temperature and sea-surface temperature (SST) anomalies (*7*) for the period from 1981 to 1993 (Fig. 2). The general pattern has been one of cooling over the oceans and warming over the continents. The North Pacific basin temperature anomalies, with warming along the west coast of North America and Alaska and cooling in the central North Pacific, have been linked to a substantial decadal change in the atmospheric circulation, which corresponded to a deepened eastward-shifted Aleutian low pressure system during the winter half of the year and lasted throughout most of the 1980s (*8*, *9*). Changes in the mean flow were accompanied by a southward shift in the storm tracks and associated synoptic eddy activity (*9*) and in surface ocean sensible and latent heat fluxes (*10*). It has been hypothesized that the Pacific decadal time scale variation has its origin in the tropics (*9*), and several modeling studies have confirmed that North Pacific atmospheric circulation changes are controlled in part by anomalous tropical Pacific SST forcing (*11*, *12*).

Decadal changes in the atmospheric circulation and lower tropospheric temperatures during winter over the North Atlantic and adjacent land areas, however, do not appear to be as strongly influenced by tropical Pacific SST variability (*12*, *13*). The anomalous coldness over the past decade near Greenland and the eastern Mediterranean, and the very warm conditions over Scandinavia, northern Europe, the former Soviet Union, and much of central Asia (Fig. 2), are more strongly linked to the recent behavior of the NAO. To isolate the important coupled modes of variability between the SLP and surface temperature and

SST fields, I applied singular value decomposition (SVD) analysis (*14*) to the temporal covariance matrix between a data set of 95 winters (1899 to 1993) consisting of seasonal mean SLP anomalies and concurrent SST and surface land temperature anomalies. The temperature data set is the same as that used to construct Fig. 2, whereas the SLP data have been carefully evaluated and corrected for errors (*15*). Because the signature of the NAO is strongly regional (Fig. 1B), a domain of 20°N to 80°N and 90°W to 40°E was selected for the SVD analysis.

The first set of singular vectors correspond to the NAO and explain nearly 75% of the total squared covariance. The changes in SLP associated with the first SVD mode (Fig. 3B) confirm that the stations used to construct the NAO index in Fig. 1A are near the main opposite centers of the teleconnection. The correlation coefficient between the expansion coefficients of the first SLP vector and the NAO time series (Fig. 1A) is 0.91 from 1899 to 1993. The similarity between the departure patterns of temperature (Fig. 3A) and the decadal anomalies over the North Atlantic and surrounding landmasses (Fig. 2) suggests that the recent temperature anomalies over these regions are strongly related to the persistent and exceptionally strong positive phase of the NAO index since the early 1980s.

Changes in the mean circulation patterns over the North Atlantic are accompanied by pronounced shifts in the storm tracks and associated synoptic eddy activity (*16*). Changes in the mean and eddy components of the flow affect the transport and convergence of atmospheric moisture and can, therefore, be directly tied to changes in regional precipitation. The atmospheric moisture budget cannot be adequately computed before 1979 because of the lack of high-quality global analyses. To provide an analogy to the low-frequency changes evident in the NAO index (Fig. 1A), I compared low or near-normal NAO winters with very high NAO winters using composites of the global analyses produced by the European Centre for Medium Range Weather Forecasts (ECMWF), which are considered to be of sufficient quality to adequately evaluate the large-scale moisture budget (*17*). For the low or normal NAO composite, the average December through March ECMWF analyses for the winters 1979, 1985, 1986, 1987, and 1988 were used. Only three of these winters have negative index values, resulting in a composited index value of -0.6 ± 0.8. The high NAO composited index is 3.5 ± 0.9, determined from the average of the 1983, 1989, 1990, 1992, and 1993 winter indices.

Vector plots of the vertically integrated total moisture transport for both the high and the normal-low NAO composites (Fig. 4) show that during times of a high NAO index, the axis of maximum moisture transport shifts to a more southwest-to-northeast orientation across the Atlantic and extends much farther to the north and east onto northern Europe and Scandinavia. A significant reduction of the total atmospheric moisture transport occurs over parts of southern Europe, the Mediterranean, and north Africa.

It is the divergence of the moisture transport, however, that determines the excess of precipitation over evaporation. Evaporation (E) exceeds precipitation (P) over much of Greenland (Fig. 4C) during high NAO winters, especially in the south where changes are on the order of 1 mm day^{-1}. Together with the low-frequency changes evident in the NAO index (Fig. 1A), these results are consistent with observational and modeling evidence of a declining precipitation rate over much of the Greenland Ice Sheet over the past two decades (*18*). During high NAO index winters, drier conditions occur over much of central and southern Europe and the Mediterranean, whereas enhanced moisture flux convergence occurs from Iceland through Scandinavia. The increases in

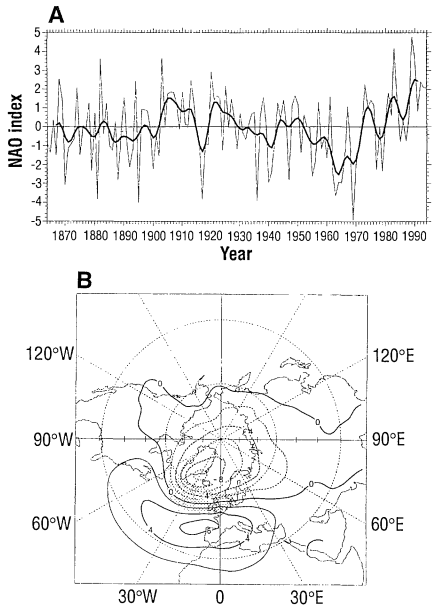

Fig. 1. (**A**) Winter (December through March) index of the NAO based on the difference of normalized pressures between Lisbon, Portugal, and Stykkisholmur, Iceland, from 1864 through 1994. The SLP anomalies at each station were normalized by division of each seasonal pressure by the long-term mean (1864 to 1994) standard deviation. The heavy solid line represents the meridional pressure gradient smoothed with a low-pass filter with seven weights (1, 3, 5, 6, 5, 3, and 1) to remove fluctuations with periods less than 4 years. (**B**) Difference in SLP between years with an NAO index >1.0 and those with an index <−1.0 (high index minus low index winters) since 1899. The contour increment is 2 mbar; negative values are dashed. Stippling indicates where the composited surface geostrophic zonal wind difference is greater than 8 m s^{-1}.

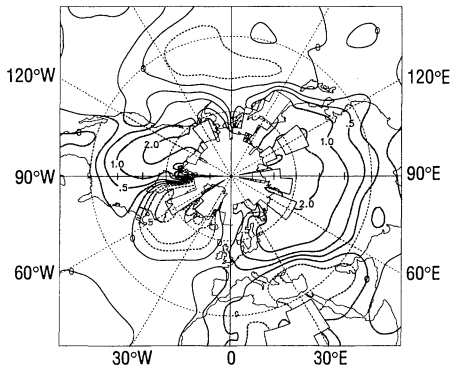

Fig. 2. Average surface temperature and SST anomalies of 13 winters (1981 through 1993, December through March), expressed as departures from the 1951 through 1980 mean. Negative anomalies less than −0.25°C are dashed, and positive anomalies greater than 0.25°C are indicated by solid contours. Regions of insufficient data are not contoured.

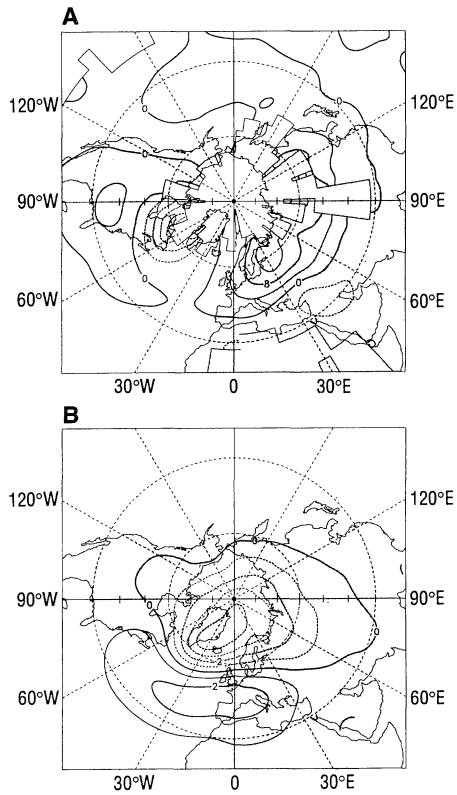

Fig. 3. Geographical patterns of the hemispheric (**A**) surface temperature and SST and (**B**) SLP departures corresponding to a unit standard deviation of the expansion coefficients of the first SLP vector. Negative departures are dashed, and regions of insufficient data are not contoured. The contour increment is 4×10^{-1}°C in (A) and 1 mbar in (B). The SLP-temperature temporal covariance matrix was computed from unnormalized winter (December through March) data over the period from 1899 through 1993.

wintertime precipitation over Scandinavia may be related to recent positive mass balances in the maritime glaciers of southwest Norway (*19*).

Long-term station records of wintertime precipitation (Table 1) support the evaporation minus precipitation ($E - P$) patterns (Fig. 4C). Correlations between the NAO index (Fig. 1A) and the station data are of greatest magnitude where the $E - P$ patterns are largest and statistically significant, whereas stations that exhibit low correlations (not listed here) are mostly located in regions where the $E - P$ map shows little signal. The main disagreement between Table 1 and Fig. 4C is that the strongest negative correlations are found at stations throughout the Azores, Portugal, Spain, and northwest Africa, whereas weaker and statistically insignificant atmospheric moisture flux divergence is indicated throughout these areas during high NAO index winters in the ECMWF data. The differences in precipitation rates between winters in which the NAO index exceeded 1.0 and winters in which the index was less than −1.0 (Table 1) also agree well with the $E - P$ patterns. They provide further evidence that the recent, decade-long winter dry conditions over southern Europe and the Mediterranean, and the wet anomalies from Iceland eastward through Scandinavia (*20*), are related to the persistent positive phase of the NAO.

The above analysis of changes in surface temperatures, precipitation, winds, and other measures of the atmospheric circulation reveals coherent, long-lived coupled variations on a regional scale. Evidence for large and rapid fluctuations in the climate of the Atlantic abound in historical and proxy records. Recent analyses of Greenland ice-core data, for instance, have revealed abrupt changes in the climate of the North Atlantic at decadal time scales (*21*) that may be related to fluctuations in the NAO (*22*). Interannual fluctuations in surface ocean conditions over the North Atlantic are largely governed by wind-induced changes in the air-sea energy fluxes, whereas interdecadal variations also involve changes in the ocean circulation (*23*). Prolonged periods with anomalous atmospheric circulation patterns associated with the NAO (Fig. 1A) alter the amount of heat extracted from the ocean by the atmosphere and the fresh water input to the ocean through changes in $E - P$, the melting of sea ice, and continental runoff and therefore are likely to affect the rate of deep water formation in the North Atlantic. Significant temperature variability on decadal time scales has been observed at depth in the ocean (*24*), but there are insufficient observations to determine what changes have occurred in the ocean thermohaline circulation.

The large warm wintertime anomalies

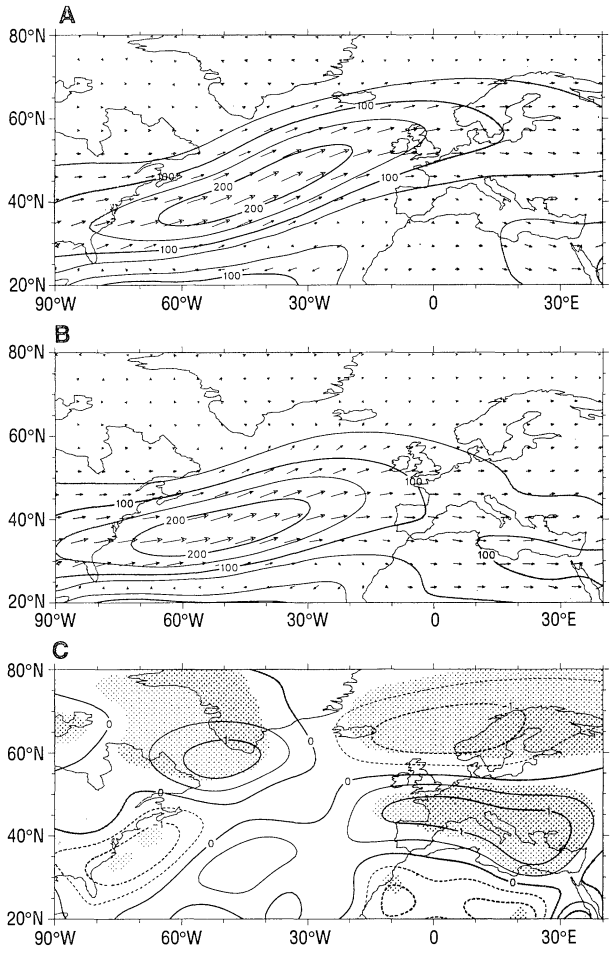

Fig. 4. Vectors of the vertically integrated moisture transports for (**A**) high NAO index winters and (**B**) normal or low NAO index winters. Evaporation minus precipitation computed from the atmospheric moisture budget for high minus normal or low NAO index winters is shown in (**C**). The contour interval of the magnitudes is 50 kg m^{-1} s^{-1} in (A) and (B). The contour interval in (C) is 0.5 mm day^{-1}, and the stippling indicates values significantly different from 0 at the 5% level with the use of a *t* test.

Table 1. Stations (latitude, longitude) that contain records of December through March precipitation for at least 40 years. The correlation coefficients between precipitation and the NAO index [*r*(NAO,*P*)] and the total number of winters (*n*) that were included in the correlations are indicated. Also indicated are the mean precipitation rates $\bar{P}$ over the total number of winters (*n*) and the differences in precipitation rates between winters with an NAO index >1.0 and those with an index <−1.0. One asterisk indicates statistical significance at the 5% level, and two indicate significance at the 1% level.

Station	*r*(NAO,*P*)	Years	$\bar{P}$ (mm day^{-1})	ΔP (mm day^{-1})
Bergen (60.4°N, 5.3°E)	0.77**	72	5.8	3.6**
Stornoway (58.2°N, 6.3°W)	0.75**	63	3.5	1.4**
Tiree (56.6°N, 6.9°W)	0.67**	63	3.4	1.2**
Stavanger (58.9°N, 5.6°E)	0.66**	43	2.7	1.4**
Thorshavn (62.0°N, 6.8°W)	0.53**	116	4.8	1.1**
Lerwick (60.1°N, 1.2°W)	0.49**	63	3.6	0.8**
Reykjavik (64.1°N, 21.9°W)	0.48**	73	2.7	0.9**
Akureyri (65.7°N, 18.1°W)	0.43**	63	1.6	0.4*
Stykkisholmur (65.1°N, 22.7°W)	0.40**	117	2.2	0.7**
Haparanda (65.8°N, 24.2°E)	0.37**	130	1.2	0.4**
Karesuando (68.5°N, 22.5°E)	0.21*	115	0.6	0.1
Oslo (60.2°N, 11.1°E)	0.21*	125	1.3	0.2
Helsinki (60.3°N, 25.0°E)	0.18*	130	1.5	0.1
Paris (49.0°N, 2.5°E)	−0.19*	119	1.5	−0.3**
Frankfurt (50.1°N, 8.7°W)	−0.19*	130	1.4	−0.2*
Godthåb (64.2°N, 51.8°W)	−0.20*	100	1.1	−0.4
Jakobshavn (69.2°N, 51.1°W)	−0.21*	95	0.4	−0.1
Ivigtut (61.2°N, 48.2°W)	−0.31*	89	2.8	−0.9*
Marseille (43.5°N, 5.2°E)	−0.32**	120	1.5	−0.5**
Milan (45.4°N, 9.3°E)	−0.35**	130	2.2	−0.8**
Istanbul (41.0°N, 29.1°E)	−0.36**	64	2.7	−0.7**
Lyon (45.7°N, 5.0°E)	−0.37**	129	1.6	−0.5**
Rome (41.8°N, 12.2°E)	−0.37**	119	2.6	−0.8**
Ajaccio (41.9°N, 8.8°E)	−0.48**	42	2.2	−1.1**
Ponta Delgado (37.8°N, 25.7°W)	−0.49**	98	3.2	−1.1**
Belgrade (44.8°N, 20.5°E)	−0.50**	94	1.4	−0.6**
Casablanca (33.6°N, 7.7°W)	−0.61**	82	2.0	−1.1**
Lisbon (38.8°N, 9.1°W)	−0.64**	130	3.0	−1.8**
Madrid (40.4°N, 3.7°W)	−0.69**	129	1.3	−1.0**

over the middle- and high-latitude continents over the past decade (Fig. 2) resemble some results obtained by coupled atmosphere-ocean models forced with steadily increasing atmospheric greenhouse gases (*25*), and evidence suggests that the recent warming may be related to increasing tropical ocean temperatures that have led to an enhancement of the tropical hydrologic cycle (*12*, *26*). However, significant decade-long changes in the atmospheric circulation, and in the NAO in particular, have contributed substantially to the regional warming, complicating the interpretation of the climate system response to increased greenhouse gas forcing. Decadal variability in the NAO has become especially pronounced since about 1950 (Fig. 1A), but the causes for such variability in the Atlantic are not clear. The relation of the NAO to greenhouse gas forcing and possible links to coherent variations in tropical Atlantic SSTs (*27*) need to be examined, along with how well climate models simulate the NAO and its recent variations.

REFERENCES AND NOTES

1. G. T. Walker and E. W. Bliss, *Mem. R. Meteorol. Soc.* **44**, 53 (1932); H. van Loon and J. C. Rogers, *Mon. Weather Rev.* **106**, 296 (1978); J. M. Wallace and D. S. Gutzler, *ibid.* **109**, 784 (1981); A. G. Barnston and R. E. Livezey, *ibid.* **115**, 1083 (1987); Y. Kushnir and J. M. Wallace, *J. Atmos. Sci.* **46**, 3122 (1989). An empirical orthogonal function analysis reveals that the NAO is the dominant mode of variability of the surface atmospheric circulation in the Atlantic and accounts for more than 36% of the variance of the mean December to March SLP field over the region from 20°N to 80°N and 90°W to 40°E during 1899 through 1994. Barnston and Livezey show that the oscillation is present throughout the year in monthly mean data but that it is most pronounced during winter.
2. J. C. Rogers, *J. Clim. Appl. Meteorol.* **24**, 1303 (1985).
3. H. H. Lamb and A. I. Johnson, "Secular variations of the atmospheric circulation since 1750," in *Geophys. Mem.* vol. 110 [Her Majesty's Stationery Office (HMSO), London, 1966]; H. H. Lamb, "British Isles weather types and a register of daily sequence of circulation patterns, 1861–1971," in *Geophys. Mem.* vol. 116 (HMSO, London, 1972); T. J. Makrogiannis, A. A. Bloutsos, B. D. Giles, *J. Climatol.* **2**, 159 (1982); D. E. Parker and C. K. Folland, *Meteorol. Mag.* **117**, 201 (1988).
4. H. van Loon and J. Williams, *Mon. Weather Rev.* **104**, 636 (1976).
5. T. Moses *et al.*, *J. Climatol.* **7**, 13 (1987).
6. K. E. Trenberth, in *Earth System Responses to Global Change: Contrasts Between North and South America*, H. A. Mooney, E. R. Fuentes, B. I. Kronberg, Eds. (Academic Press, New York, 1993), pp. 35–59.
7. The data consist of land surface temperature data from the University of East Anglia [P. D. Jones, *J. Clim.* **1**, 654 (1988)] blended with SST data from the United Kingdom Meteorological Office [M. Bottomley, C. K. Folland, J. Hsiung, R. E. Newell, D. E. Parker, "Global ocean surface temperature atlas" (UK Meteorological Office, London, 1990)].
8. T. Nitta and S. Yamada, *J. Meteorol. Soc. Jpn.* **67**, 375 (1989); K. E. Trenberth, *Bull. Am. Meteorol. Soc.* **71**, 988 (1990).
9. K. E. Trenberth and J. W. Hurrell, *Clim. Dynam.* **9**, 303 (1994).
10. D. R. Cayan, *J. Clim.* **5**, 354 (1992).
11. A. Kitoh, *J. Meteorol. Soc. Jpn.* **69**, 271 (1991); T.-C. Chen, H. van Loon, K.-D. Wu, M.-C. Yen, *ibid.* **70**, 1137 (1992); N. E. Graham, *Clim. Dynam.* **9**, 135 (1994); A. J. Miller, D. R. Cayan, T. P. Barnett, N. E. Graham, J. M. Oberhuber, *ibid.*, p. 287.
12. A. Kumar *et al.*, *Science* **266**, 632 (1994).
13. N. E. Graham *et al.*, *J. Clim.* **7**, 1416 (1994); N.-C. Lau and M. J. Nath, *ibid.*, p. 1184.
14. C. S. Bretherton *et al.*, *ibid.* **5**, 541 (1992).
15. K. E. Trenberth and D. A. Paolino, *Mon. Weather Rev.* **108**, 855 (1980).
16. J. C. Rogers, *J. Clim.* **3**, 1364 (1990); J. W. Hurrell, *J. Atmos. Sci.* **52**, 2286 (1995).
17. K. E. Trenberth, *Nat. Ctr. Atmos. Res. Tech. Note NCAR/TN-373+STR* (National Center for Atmospheric Research, Boulder, CO, 1992); ——— and C. J. Guillemot, *J. Clim.*, in press. The ECMWF data were truncated at 21 wave numbers with a spherical harmonic representation and were available at seven vertical levels. The moisture budget was computed with the vertically integrated equation for conservation of water vapor, ignoring the role of liquid water in the atmosphere and the local rate-of-change term

$$\nabla \cdot \frac{1}{g} \int_0^{P_s} q\mathbf{v}dp = E - P$$

where q is the specific humidity, $\mathbf{v}$ is the horizontal vector wind, and p is pressure; s denotes surface pressure, and g represents gravity.
18. D. H. Bromwich, F. M. Robasky, R. A. Keen, J. F. Bolzan, *J. Clim.* **6**, 1253 (1993).
19. World Glacier Monitoring Service (WGMS), Glacier Mass Balance Bulletin no. 3, 1992–1993 (Zurich, 1994).
20. National Oceanic and Atmospheric Administration (NOAA), Climate Assessment: A Decadal Review 1981–1990 (Government Printing Office, Washington, DC, 1991). Seasonal precipitation anomaly distributions are available from NOAA Annual Climate assessments, from Climate System Monitoring (CSM) monthly bulletins produced by the World Climate Programme, and from NOAA monthly climate diagnostics bulletins.
21. C. U. Hammer *et al.*, *Radiocarbon* **28**, 284 (1986); W. Dansgaard *et al.*, *Nature* **339**, 532 (1989); K. C. Taylor *et al.*, *ibid.* **361**, 432 (1993); R. B. Alley *et al.*, *ibid.* **362**, 527 (1993).
22. L. K. Barlow *et al.*, *Geophys. Res. Lett.* **20**, 2901 (1993).
23. J. Bjerknes, *Adv. Geophys.* **10**, 1 (1964); C. Deser and M. L. Blackmon, *J. Clim.* **6**, 1743 (1993); Y. Kushnir, *ibid.* **7**, 141 (1994).
24. S. Levitus *et al.*, *Science* **266**, 96 (1994).
25. Intergovernmental Panel on Climate Change (IPCC), *Climate Change 1992: The Supplementary Report to the IPCC Scientific Assessment*, J. T. Houghton, B. A. Callander, S. K. Varney, Eds. (Cambridge Univ. Press, Cambridge, 1992).
26. N. E. Graham, *Science* **267**, 666 (1995).
27. N.-C. Lau and M. J. Nath, *J. Clim.* **3**, 965 (1990).

28. The ECMWF data were provided by ECMWF. The comments of two anonymous reviewers helped improve the manuscript. Special thanks to K. Trenberth and H. van Loon for their scientific guidance and useful comments and suggestions. The National Center for Atmospheric Research is sponsored by NSF.

20 March 1995; accepted 30 May 1995

Rescue of the *En-1* Mutant Phenotype by Replacement of *En-1* with *En-2*

Mark Hanks,* Wolfgang Wurst,† Lynn Anson-Cartwright, Anna B. Auerbach,‡ Alexandra L. Joyner‡§

The related mouse *Engrailed* genes *En-1* and *En-2* are expressed from the one- and approximately five-somite stages, respectively, in a similar presumptive mid-hindbrain domain. However, mutations in *En-1* and *En-2* produce different phenotypes. *En-1* mutant mice die at birth with a large mid-hindbrain deletion, whereas *En-2* mutants are viable, with cerebellar defects. To determine whether these contrasting phenotypes reflect differences in temporal expression or biochemical activity of the En proteins, *En-1* coding sequences were replaced with *En-2* sequences by gene targeting. This rescued all *En-1* mutant defects, demonstrating that the difference between *En-1* and *En-2* stems from their divergent expression patterns.

The mouse *Engrailed* (*En*) genes *En-1* and *En-2* are the murine members of a large conserved gene family related to the *Drosophila* segmentation gene *engrailed* (*en*). All *En* genes encode proteins that contain a homeodomain as well as four small, highly conserved regions (*1*). However, outside these regions, En proteins share little identity across the phyla. Overall, En-1 and En-2 proteins share approximately 55% amino acid identity with each other and approximately 35% identity with *Drosophila* En protein.

En-1 expression is first detected during mouse embryogenesis at the one-somite stage, in cells of the anterior neural folds. *En-2* expression, which occurs in a similar region, initiates at the five-somite stage but does not fully overlap with *En-1* until approximately eight somites have formed (*2*). Expression of both genes continues in cells of the ventricular layer of this presumptive mid-hindbrain region. At 9.5 days post coitus (dpc), *En-1* expression

Division of Molecular and Developmental Biology, Samuel Lunenfeld Research Institute, Mt. Sinai Hospital, Toronto M5G 1X5, Canada.

*Present address: Procter and Gamble Pharmaceuticals, Miami Valley Laboratories, Cincinnati, OH 45253–8707, USA.

†Present address: GSF Research Center, Institute for Genetics, Ingolstaedter Landstrasse 1D-85758, Oberschleissheim-Munich, Germany.

‡Present address: Developmental Genetics Program, Skirball Institute of Biomolecular Medicine, New York University Medical Center, 540 First Avenue, New York, NY 10016, USA.

§To whom correspondence should be addressed.